Proceedings of the ASME 2010 3rd Joint US-European Fluids Engineering Summer Meeting and 8th International Conference on Nanochannels, Microchannels, and Minichannels
FEDSM-ICNMM2010
August 1-5, 2010, Montreal, Canada

FEDSM-ICNMM2010-30536

EXPERIMENTAL AND NUMERICAL STUDY OF THE THREE DIMENSIONAL INSTABILITIES IN THE WAKE OF A BLUNT TRAILING EDGE PROFILED BODY

Arash Naghib Lahouti
The University of Western Ontario
London, Ontario, Canada

Lakshmana Sampat Doddipatla
The University of Western Ontario
London, Ontario, Canada

Horia Hangan
The University of Western Ontario
London, Ontario, Canada

Kamran Siddiqui
The University of Western Ontario
London, Ontario, Canada

ABSTRACT

The wake of nominally two dimensional bluff bodies is dominated by von Kármán vortices, which are accompanied by three dimensional instabilities beyond a threshold Reynolds number. These three dimensional instabilities initiate as dislocations in the von Kármán vortices near the trailing edge, which evolve into pairs of counter-rotating vortices further downstream. The wavelength of the three dimensional instabilities depends on profile geometry and Reynolds number. In the present study, the three dimensional wake instabilities for a blunt trailing edge profiled body, composed of an elliptical leading edge and a rectangular trailing edge, have been studied in Reynolds numbers ranging from 500 to 1200, based on the thickness of the body. Numerical simulations, Laser Induced Fluorescence (LIF) flow visualization, and Particle Image Velocimetry (PIV) methods have been used to identify the instabilities. Proper Orthogonal Decomposition (POD) has been used to analyze the velocity field data measured using PIV. The results confirm the existence of three dimensional instabilities with an average wavelength of 2.0 to 2.5 times thickness of the body, in the near wake. The findings are in agreements with the values reported previously for different Reynolds numbers, and extend the range of Reynolds numbers in which the three dimensional instabilities are characterized.

KEYWORDS

Blunt Trailing Edge Profiled Body, Wake Instability, Numerical Simulation, Flow Visualization, Particle Image Velocimetry, Streamwise Vortex

NOMENCLATURE

a	POD time varying coefficient
b	span of the blunt trailing edge profiled body
d	thickness of the blunt trailing edge profiled body
E_M	Relative cumulative energy of the first M POD modes
f_S	vortex shedding frequency
H	width wake, defined as $d + 2\theta$
l	chord length of the profiled body
M	number of POD modes used for reconstruction
N	number of samples in time, number of POD modes
Re	Reynolds number
Ro	Roshko number, defined as $\mathrm{Re}.St$
St	Strouhal number
t	time
T_S	vortex shedding period
u	velocity
θ	boundary layer momentum thickness
φ	POD mode
λ	wavelength of wake instabilities, POD eigenvalues
ω	vorticity

Subscripts and Superscripts

n	n-th POD mode
x	streamwise direction
z	spanwise direction
∞	free stream
$*$	reconstructed

1. INTRODUCTION

The wake of two-dimensional bluff bodies is accompanied by three dimensional instabilities when Reynolds number is higher than a certain threshold. These three dimensional instabilities, which manifest as pairs of counter-rotating streamwise vortices connecting the primary von Kármán vortices, are dependent on several parameters, including Reynolds number, free stream turbulence, and the boundaries at the two ends of the three dimensional bluff body, as pointed out qualitatively in a review by Oertel [1].

The wavelength of the three dimensional wake instabilities is also dependent on the geometry of the bluff body, and a broad range of wavelengths have been reported for different profile geometries.

A quantitative investigation of three dimensional instabilities in the wake of a circular cylinder for various Reynolds numbers is presented by Williamson [2]. Williamson distinguishes two prominent three dimensional instability modes with different spanwise wavelengths (λ_z) and vorticity structures, which might exist individually or mutually depending on the flow conditions. These two modes, known as Mode A and Mode B, have spanwise wavelengths of $\lambda_z = 3d \sim 5d$, and $\lambda_z = 1d$, respectively, where d is the diameter of the circular cylinder. According to Williamson [2], the Mode A instability emerges at $\mathrm{Re}(d) = 180 - 194$, where d is the diameter of the circular cylinder. The Mode B instability occurs at a higher Reynolds number, in the range of $\mathrm{Re}(d) = 230 - 250$. The three dimensional wake instability wavelengths for the circular cylinder are verified by several other researchers, including Brede et al. [3].

In case of a very long and thin flat plat with no leading edge effects, Julien et al. [3] report a prominent spanwise wavelength of $\lambda_z = 12H$ at $\mathrm{Re}(H) = 200$ for the secondary wake instabilities, where H is the width of the wake at the trailing edge.

For a square cylinder geometry, Dobre and Hangan [5] report a spanwise instability wavelength of $\lambda_z = 2.4d$ at $\mathrm{Re}(d) = 2.2 \times 10^4$, based on a wavelet analysis of their simultaneous hotwire measurements in the intermediate wake region ($x/d = 26$).

A similar spanwise instability wavelength has been reported by El Gammal and Hangan [6] in the near wake region of a divergent trailing edge airfoil with a trailing edge thickness to chord ratio of 1.8%. Based on their hotwire measurements, they report a spanwise instability wavelength of $\lambda_z = 2.4d$ at $\mathrm{Re}(d) = 1.3 \times 10^4$, where d is the trailing edge thickness.

The case of a blunt trailing edge profiled body, which comprises a flat plate with an elliptical leading edge, is especially interesting as it represents a simplified blunt trailing edge airfoil, and also because it provides the desired upstream boundary layer velocity profile at the trailing edge without the uncontrollable effects of forced separation-reattachment associated with sharp corners of a square leading edge, or the partial separation due to curvature or divergence of the trailing edge, as highlighted in [6].

Ryan et al. [7] have reported two prominent three dimensional instability modes for this profile at low Reynolds numbers ranging from $\mathrm{Re}(d) = 220$ to $\mathrm{Re}(d) = 700$. Based on a Floquet stability analysis, they have identified two instability modes, named Mode A and Mode B', which are similar in vorticity structure to the modes A and B identified for a circular cylinder in the experimental work of Williamson [2], respectively. While the spanwise wavelengths of Mode A for this profile is similar to that of a circular cylinder ($\lambda_z = 3.5d$), Mode B' has a larger wavelength of $\lambda_z = 2.2d$. Their analysis indicates for chord to thickness ratios (l/d) equal to, or greater than 12.5, the critical $\mathrm{Re}(d)$ for Mode B', which is close to 400, is less than the critical $\mathrm{Re}(d)$ for Mode A, which is 600. Therefore, Mode B', with a spanwise wavelength of $\lambda_z = 2.2d$, is expected to be the first three dimensional wake instability to be observed in experiments.

Inducing three dimensional instabilities into the wake of a bluff body is a well known wake flow control approach when disorganization of the regular structure of von Kármán vortices is intended.

Previous studies have shown that amplification of the secondary wake instabilities with a spanwise wavelength close to the natural wavelength of the instabilities can result in significant reduction of aerodynamic forces. Considering its unique aerodynamic characteristics, the blunt trailing edge profiled body geometry has been commonly used as a platform for evaluation of this flow control approach. Examples of the implementation of this approach for the blunt trailing edge profiled body at high Reynolds numbers in the range of $\mathrm{Re}(d) = 2 \times 10^4 \sim 8 \times 10^4$ can be found in the works of Bearman and Tombazis [8,9], Park et al. [10], and Doddipatla et al. [11].

The present study intends to extend the range of Reynolds numbers at which the three dimensional instabilities in the wake of the blunt trailing edge profiled body are studied. The extended range in which the three dimensional wake instabilities are characterized can serve as a basis for designing flow control mechanisms that are able to retain their effectiveness in a broader range of operating conditions, by inducing three dimensional instabilities at the appropriate wavelength for each Reynolds numbers.

Three methods have been used herein to identify and quantify the three dimensional instabilities in the wake of the blunt trailing profiled body. They include Computational Fluid Dynamics (CFD) simulations, Planar Laser Induced Fluorescence (LIF) flow visualizations, and velocity field data measurement using Particle Image Velocimetry (PIV), analyzed

using Proper Orthogonal Decomposition (POD). The simulations and experiments are carried out at Reynolds numbers ranging from $\mathrm{Re}(d) = 500$ to $\mathrm{Re}(d) = 1200$.

2. NUMERICAL SIMULATION

The blunt trailing edge profiled body geometry studied herein, which has a thickness to chord ratio of $l/d = 12.5$, is similar to the one studied in [7-11]. It consists of an elliptical nose with a major to minor diameter ratio of 5:1, followed by a rectangular section with a 10:1 length to thickness ratio, as shown in Fig. 1.

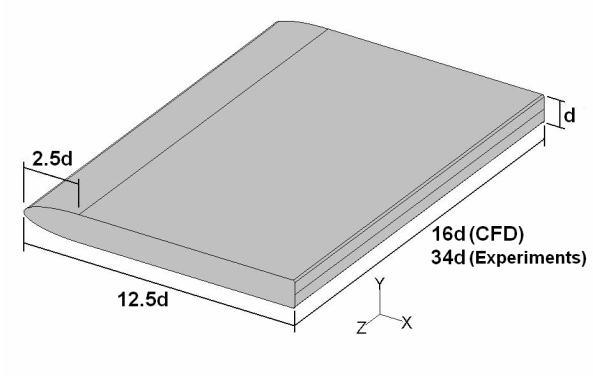

FIGURE 1: GEOMETRY AND DIMENSIONS

The solution domain is defined as a hexahedral volume surrounding the profiled body. The domain extends 60*d* behind, 24*d* in front, and 24*d* from the upper and lower surfaces of the body (Fig. 2a). The distances between the solid surfaces of the body and the domain boundaries are selected based on a number of trials using various domain sizes, so that the perturbations caused by the body diminish to a level that would not cause numerical inconsistencies, such as convergence problems, when they reach the boundaries.

The region surrounding the solid walls of the body, as well as the region covering the near wake (*3d* downstream from the base of the body) is discretized using a boundary layer-type structured grid of hexahedral cells, which are refined towards the solid surfaces. The remaining part of the solution domain, which encompasses the inner region, is discretized using an unstructured grid of tetrahedral cells. The grid size has been previously increased in steps of +25% until grid independence in terms of surface pressure distribution is achieved. A close up of the final hybrid grid, which has a total of 1.05×10^6 cells, is shown in Fig. 2b.

The segregated implicit scheme based on the SIMPLE algorithm, which is available in the commercial CFD program FLUENT, has been used for solution of the governing equations in three dimensions. Details of the numerical solution procedure are provided in the CFD code's documentation [12].

Temporal discretization is carried out using a time step size of $1/250\,T_S$, where T_S is the predicted shedding period of von Kármán vortices at each Reynolds number. The temporal duration covered by each numerical simulation is equivalent to 50 vortex shedding periods ($50T_S$) approximately, following the development of periodic behavior in the wake.

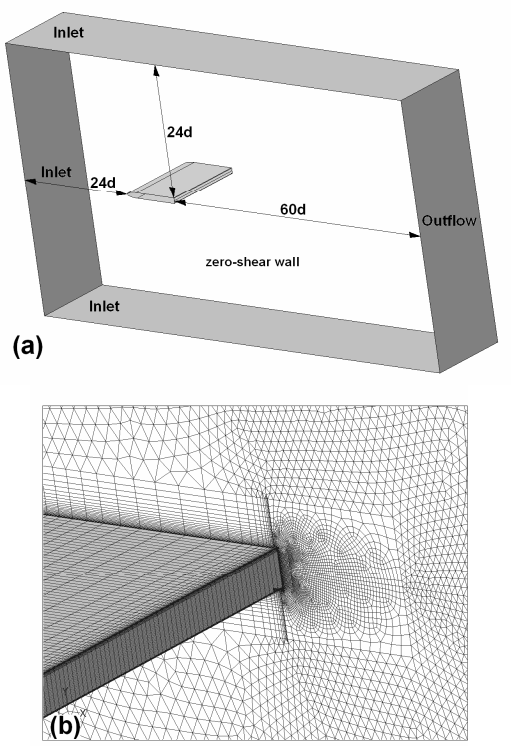

FIGURE 2: THE SOLUTION DOMAIN AND BOUNDARIES (a), AND DETAIL OF THE GRID IN THE BASE REGION

3. FLOW VISUALIZATION

Flow visualizations have been carried out using planar Laser Induced Fluorescence (LIF) technique. The experiments have been performed in a closed test section water tunnel able to generate a maximum free stream velocity of 0.2m/s in a 0.6m (w) x 0.3m (h) test section, using a model with the same profile geometry as the one modeled in the numerical simulations. The experimental model has a total span of b = 0.6m, which is equivalent to 48d. However, the centre 34*d* portion of the span, which is bounded by two endplates, has been used for visualization. The endplates isolate the body from the effects of the boundary layers on the sidewalls of the tunnel, as well as the dye supply system tubing. The Rhodamine 6G fluorescent dye is introduced to the wake flow through a thin spanwise slot on the lower surface of the body, located 1*d* upstream of the trailing edge. The measurement area is illuminated by a light sheet generated using an Nd-YAG pulse laser with a wavelength of 532nm. Images are captured by a CCD camera

through a 550nm filter, which filters the laser light, but passes 560 nm light generated by the fluorescent dye. Fig. 3 shows a schematic drawing of the experimental setup.

Visualizations have been carried out in the vertical (xy) plane located at mid-span at $\mathrm{Re}(d) = 550$, 850, 1150, and 1320, in order to determine the principal characteristics of the von Kármán vortex street, and in the horizontal (xz) plane located at $y/d = -0.5$, which corresponds to the lower trailing edge of the profiled body, at $\mathrm{Re}(d) = 550$, in order to study the three dimensional wake instabilities.

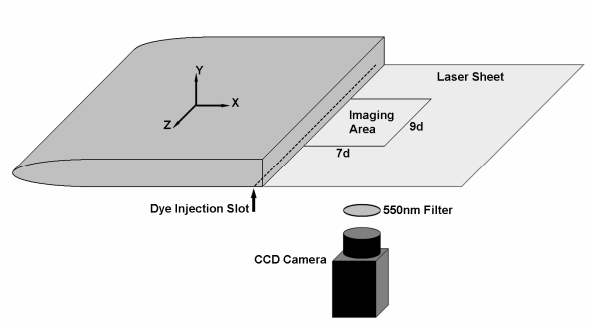

FIGURE 3: SCHEMATIC DRAWING OF THE EXPERIMENTAL SETUP FOR LIF ANDPIV EXPERIMENTS. THE LASER SHEET SHOWN CORRESPONDS TO y/d=-0.5. THE FILTER IS NOT USED IN PIV EXPERIMENTS.

4. VELOCITY FIELD MEASUREMENT AND ANALYSIS

Velocity field measurements have been carried out at $\mathrm{Re}(d) = 550$, 850, and 1200 using Particle Image Velocimetry (PIV) technique, utilizing the same experimental equipment and setup as the ones described in the flow visualization section and shown in Fig.3.

Two sets of measurements are carried out for each Reynolds number, in two parallel horizontal (xz) planes corresponding to the midplane ($y/d = 0$), and lower trailing edge ($y/d = -0.5$) locations. For each set, 3000 image pairs have been recorded in a measurement area with the approximate dimensions of $9d \times 7d$, with a sampling rate of 15 image pairs per second. (Fig.3)

Each image pair, which includes two 1600×1200 pixel images, has been processed to generate an array of 99×74 velocity vectors in the measurement area.

The velocity vector field data are then analyzed using the Proper Orthogonal Decomposition (POD) technique, also known as Principal Component Analysis (PCA). This technique projects a data ensemble, which is built by acquiring N samples of a scalar or vector field variable $u_i(x_i,t)$, onto N orthogonal eigenfunctions or modes $\phi^n(x_i)$, so that the first mode accounts for as much variability in the data as possible, and each succeeding mode accounts for as much as the remaining variability as possible. In other words, the modes obtained by the POD technique are energetically optimal, and if the first $M \le N$ POD modes are used to reconstruct the original data ensemble, the result will contain more energy than any other reconstruction carried out using any M modes obtained on any other basis.

Each POD mode $\phi^n(x_i)$ is accompanied by a time varying amplitude coefficient $a^n(t)$, and the combination of these two can be used to reconstruct the original data ensemble using:

$$u_i^*(x_i,t) = \sum_{n=1}^{M} a^n(t)\phi^n(x_i) \tag{1}$$

, in which $u_i^*(x_i,t)$ is an approximate reconstruction of the original data ensemble, generated using $M \le N$ modes.

As shown in [13], the modes $\phi^n(x_i)$ can be obtained by finding the eigenvalues and eigenfunctions in the following problem:

$$\int \langle u_i(x_i,t).u_i(x_i',t)\rangle \phi^n(x_i')dx_i' = \lambda^n \phi^n(x_i) \tag{2}$$

, in which the $\langle . \rangle$ operator represents spatial autocorrelation. The detailed procedure for discretization and solution of this problem can be found in [14] and [15]. Once the modes are obtained, the amplitude coefficients can be found by projecting the original data onto the POD modes using:

$$a^n(t) = \int u_i(x_i,t).\phi^n(x_i)dx_i \tag{3}$$

The eigenvalues λ^n in Equation 2 represent the energy contained by each mode, and can be used for sorting the modes in the order of relative energy. The unique properties of the POD technique, including orthonormality and the optimal representation of energy by the modes make it an ideal tool for filtering out the noise in a complex data ensemble, in order to reveal the often hidden, simplified underlying structures. In the present study, this technique has been used to reconstruct a simplified representation of the velocity field data, which makes it possible to identify and quantify the three dimensional wake instabilities more easily.

5. RESULTS AND DISCUSSION

Results of the numerical simulations and the experiments described in the previous sections will be analyzed in the following section in order to determine the principal characteristics of the primary wake instability (the von Kármán vortex street), and the secondary three dimensional wake instabilities, for the blunt trailing edge profiled body.

The von Kármán Vortex Street

Results of the numerical simulations and LIF flow visualizations indicate that a von Kármán vortex street is formed in the wake of the blunt trailing edge profiled body. The

vortex street can be observed in Fig.4, which shows contours of vorticity magnitude $|\omega|$ plotted at the mid-span section of the solution domain, and Fig.5, which shows LIF flow visualization images at the same section.

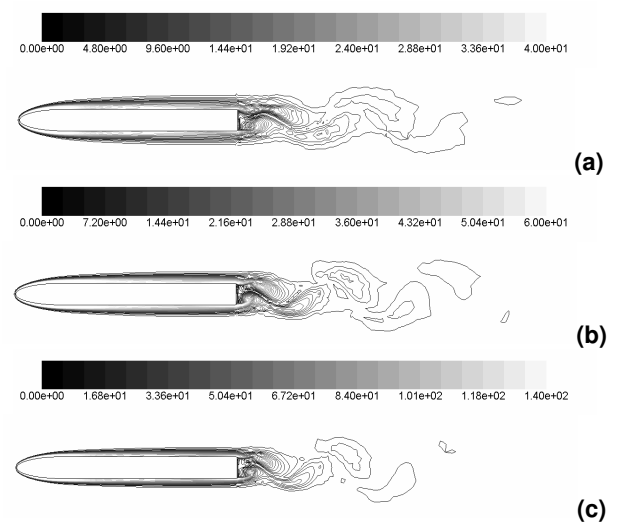

FIGURE 4. CONTOURS OF VORTICITY MAGNITUDE |ω| ON THE MID PLANE OF THE SOLUTION DOMAIN AT Re(d)=500 (a), 800 (b), and 1200 (c)

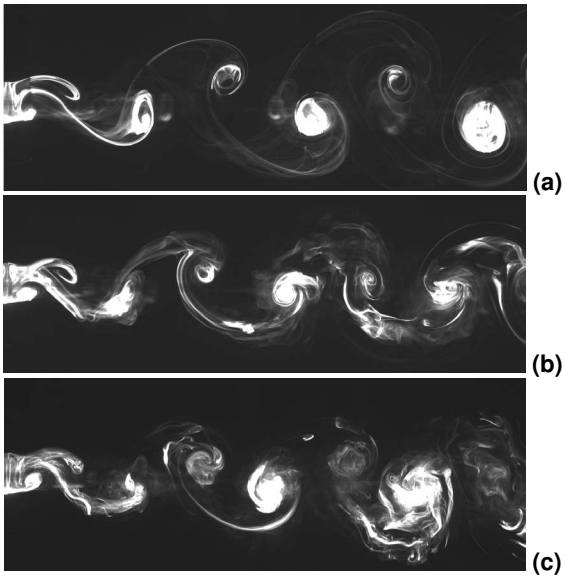

FIGURE 5. LIF VISUALIZATIONS OF THE VON KÁRMÁN VORTEX STREET AT Re(d)=550 (a), 850 (b), and 1150 (c)

The numerical simulations and LIF flow visualizations both indicate that as Reynolds number increases, the thickness of the shear layer decreases. This decrease in shear layer thickness is accompanied by a decrease in the wavelength of the primary wake instability λ_x , which can be observed Figures 4 and 5 as a smaller spacing between consecutive von Kármán vortices for higher Reynolds numbers. This observation can be verified quantitatively by comparing the values of λ_x for the Reynolds numbers at which numerical simulations or visualizations have been carried out, as shown in Fig.6. The streamwise wavelengths shown in Fig. 6 are determined by measuring the average distance of two consecutive vortices shed from one corner of the trailing edge over multiple shedding periods, in the near wake region ($x/d \le 10$), with the starting point for the measurements located approximately *4d-5d* downstream of the trailing edge. The figure also indicates a good agreement between the wavelengths obtained from the numerical simulations and those measured based on the LIF flow visualizations.

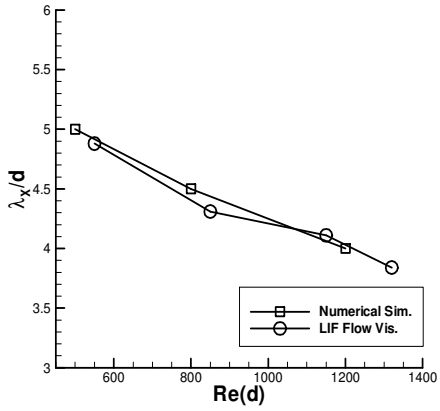

FIGURE 6. WAVELENGTH λ_X OF THE PRIMARY WAKE INSTABILITY (THE VON KAMRAN VORTEX STREET)

Considering their relatively high temporal resolution, the results of the numerical simulations have been used to determine the normalized vortex shedding frequency, which is represented by Strouhal number:

$$St = \frac{f_S d}{u_\infty} \tag{4}$$

The values of Strouhal number obtained from the numerical simulations are $St = 0.152$, 0.167, and 0.78, for $\mathrm{Re}(d) = 500$, 800, 1200, respectively. Figure 7 compares these values with the vortex shedding frequencies reported in [7], in form of variations of Roshko number with Reynolds number. Roshko number is given by:

$$Ro = \mathrm{Re}.St \tag{5}$$

It should be noted that in Reynolds number and Roshko number in Fig. 7 are expressed in terms of wake thickness H , which is defined as:

$$H = d + 2\theta \tag{6}$$

,in which θ is the boundary layer momentum thickness measured at the trailing edge of the profiled body. It can be observed in Fig.7 that the Roshko number corresponding to the numerical simulation at $\mathrm{Re}(d) = 500$ is in very close agreement with the one reported in [7], and those associated with $\mathrm{Re}(d) =$ 800 and 1200 follow the general linear trend proposed in [7] closely, suggesting that the linear relationship between $Ro(H)$ and $\mathrm{Re}(H)$ might be valid for Reynolds numbers higher than those examined in [7].

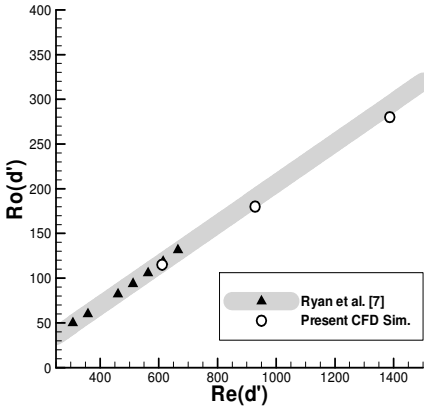

FIGURE 7. VORTEX SHEDDING FREQUENCIES EXPRESSED IN TERMS OF ROSHKO NUMBER BASED ON THE NUMERICAL SIMULATION, COMPARED WITH THE VALUES REPORTED BY RYAN ET AL. [7]

The Three Dimensional Wake Instabilities

As mentioned earlier in section 1, the three dimensional instabilities in the von Kármán vortex street are known to evolve into pairs of counter rotating streamwise vortices. Therefore, streamwise vorticity (ω_X) can be considered as an appropriate parameter for identification of the three dimensional instabilities. While experimental measurement of ω_X is challenging, a three dimensional numerical simulation of the wake flow provides field variables that can be used to study variations of ω_X.

To identify the three dimensional instabilities using the results of the numerical simulations, the spatial and temporal variations of ω_X are studied along a spanwise line located 2d downstream of the upper trailing edge ($x/d = 2, y/d = 0.5$). These variations are shown in Figs. 8a, 8b, and 8c, for $\mathrm{Re}(d) = 500$, 800, and 1200, respectively. The figure shows that for all Reynolds numbers the periodic shedding of spanwise vortices in the wake is accompanied by a streamwise vorticity component, which results from the three dimensional instability in the spanwise vortices. It can also be observed that the streamwise vorticity component alternates periodically across the span. Results for other streamwise locations are not shown here for the sake of brevity, but it should be mentioned that for each Reynolds number, a common trend of evolution and periodicity of the streamwise vorticity component has been observed at other downstream locations ranging from $x/d = 0.5$ to $x/d = 4.0$, albeit with different intensities.

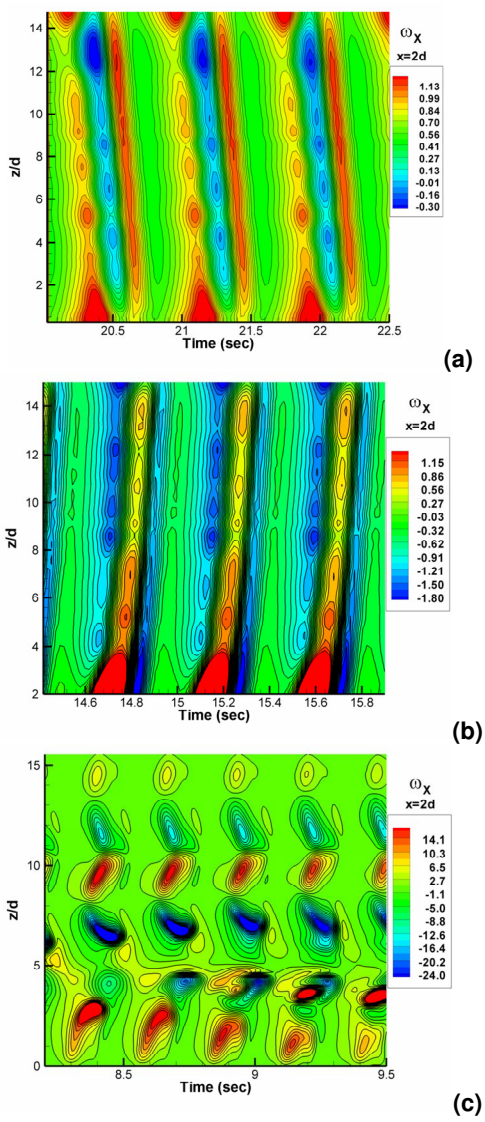

FIGURE 8. SPATIAL AND TEMPORAL VARIATIONS OF STREAMWISE VORTICITY (ωX) AT x/d=2.0, y/d=0.5, FOR Re(d)=500 (a), 800 (b), AND 1200 (c)

To determine the spanwise wavelength (λ_Z), phase-averaged plots of streamwise vorticity across the span based on the spanwise and temporal data shown in Fig.8 are generated. It should be noted that the temporal domain used for phase averaging is not limited to what is shown in Fig.8, and covers all periodic vortex shedding cycles. These plots are shown in Fig.9, which shows the phase averaged spanwise variations of ω_X at $x/d = 2$, $y/d = 0.5$ for the three Reynolds numbers studied herein. The average spanwise wavelength of the three

dimensional instabilities (λ_z), which is defined as the average spanwise distance between relative maxima or minima of streamwise vorticity ω_x can be found using the phase average plots. This distance is found to be $\lambda_z / d = 2.0$ for $\mathrm{Re}(d) = 500$ and 800. At $\mathrm{Re}(d) = 1200$, the distance between local maxima or minima ω_x is not constant in time (Fig.8c), and spanwise distances as small as 2.0d and as large as 3.5d are occasionally observed. However, the average spanwise wavelength at $\mathrm{Re}(d) = 1200$ is found to be $\lambda_z / d = 2.5d$, approximately.

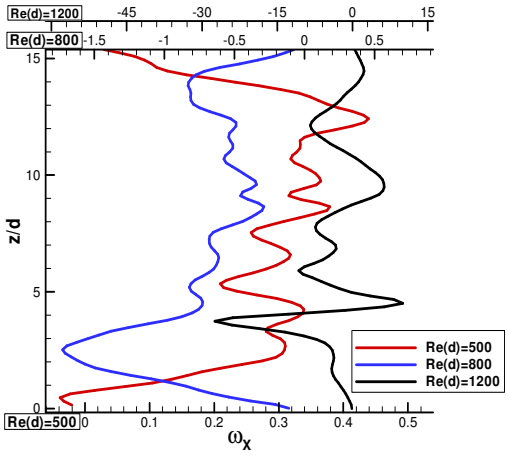

FIGURE 9. PHASE AVERAGED SPANWISE VARIATIONS OF STREAMWISE VORTICITY (ω_X) AT x/d=2.0, y/d=0.5, FOR Re(d)=500, 800, AND 1200

The evolution of the three dimensional instabilities in the von Kármán vortices into pairs of counter rotating streamwise vortices is best illustrated by the LIF flow visualizations in the horizontal (xz) plane. Figure 10 shows an LIF visualization image captured at $\mathrm{Re}(d) = 550$, with the laser sheet illuminating a horizontal (xz) plane coinciding with the lower trailing edge of the airfoil. ($y / d = -0.5$, as shown in Fig.3)

The figure clearly shows the spanwise instabilities as waves in the von Kármán vortex closest to the trailing edge of the airfoil, which are marked with (►) symbols in the figure. Further downstream, the waves evolve into pairs of counter rotating streamwise vortices, which are marked with (◄) symbols in the figure.

The LIF images can be scaled in order to determine the wavelength of the three dimensional instabilities. For example, the wavelengths observed in Fig.10 are between 1.85d and 2.5d, with an average of $\lambda_z = 2.1d$. This value, however, is based on a single snapshot, and if a statistically consistent value is intended, the wavelength should be measured in several images, possibly using an intelligent pattern recognition technique. The other challenge encountered in visualization of the three dimensional instabilities using the LIF method is the extreme dispersion of the fluorescent dye, which occurs beyond $\mathrm{Re}(d) = 550$, and makes recognition of any pattern in the images extremely difficult. This is the reason why PIV measurements of the velocity field in conjunction with the POD technique have been used to identify and quantify three dimensional instabilities experimentally.

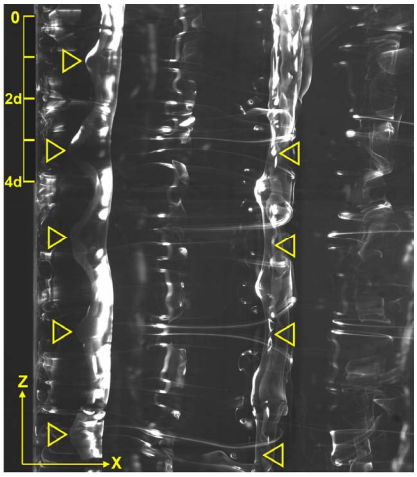

FIGURE 10. LIF VISUALIZATION IN THE HORIZONTAL PLANE AT THE LOWER TRAILING EDGE (y/d=-0.5) AT Re(d)=550. THE (►) SYMBOLS INDICATE VORTEX DISLOCATIONS DUE TO THE INSTABILITIES, AND THE (◄) SYMBOLS INDICATE PAIRS OF COUNTER-ROTATING STREAMWISE VORTICES.

As observed in Fig.10, the three dimensional instabilities initiate as streamwise dislocations of the von Kármán vortices near the trailing edge, which eventually break down into pairs of counter rotating streamwise vortices. These streamwise dislocations are accompanied by spanwise variations of the streamwise velocity component (u_x), in which the "valleys" of the dislocations (marked with (►) symbols in Fig.10) are associated with lower streamwise velocities. This phenomenon has been used to study the three dimensional instabilities based on the velocity vector field data acquired through PIV measurements.

The data have been analyzed using the POD technique described in section 4, and the POD modes have been used to reconstruct the velocity field in space and time, using Eq.1. When reconstructing a flow field using POD modes, it is important to note what proportion of the energy contained by the original data set is reproduced by the reconstructed flow field. Considering the fact that the eigenvalue λ^n represents the relative energy contained by the n-th POD mode, the relative cumulative energy of the first M POD modes (E_M) can be determined using:

$$E_M = \sum_{n=1}^{M} \lambda^n \Big/ \sum_{n=1}^{N} \lambda^n \qquad (5)$$

, in which M is the number of POD modes used for reconstruction, and N is the total number of POD modes. The relative cumulative energy of the first 500 POD modes of the streamwise velocity component (u_X), measured in the horizontal (xz) plane located at $y/d = 0$ are shown in Fig.11 for $\mathrm{Re}(d) = 550$, 850, and 1200. The figure shows the relative cumulative energy contained by any given number of POD modes is smaller at higher Reynolds numbers. This means that for higher Reynolds numbers, more energy is contained by the higher POD modes (the ones with smaller spatial and temporal scales), which is indicative of the onset of turbulence in the wake.

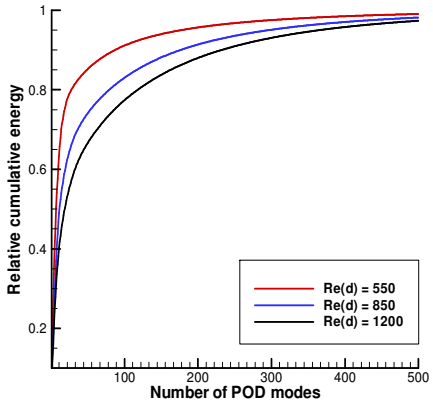

FIGURE 11. THE RELATIVE CUMLATIVE ENERGY OF THE FIRST 500 POD MODES OF U-VELOCITY MEASURED IN THE XZ PLANE LOCATED AT y/d=0

To reconstruct the u_X velocity field, the first 32 POD modes have been used. The relative cumulative energy contained by the first 32 POD modes at $\mathrm{Re}(d) = 550$, 850, and 1200 is 80%, 70%, and 60%, respectively. To illustrate the results, examples of spatial and temporal variations of u_X velocity along a spanwise line located $2d$ downstream of the trailing edge ($x/d = 2$, $y/d = 0$) are plotted in Fig.12 for the three Reynolds numbers. The figures clearly show the alternating spanwise variations of streamwise velocity, which are resulted by the streamwise dislocations of the von Kármán vortices due to the three dimensional instabilities. A similar behavior has been observed in the results obtained for other streamwise locations in the near wake region, which are not shown here.

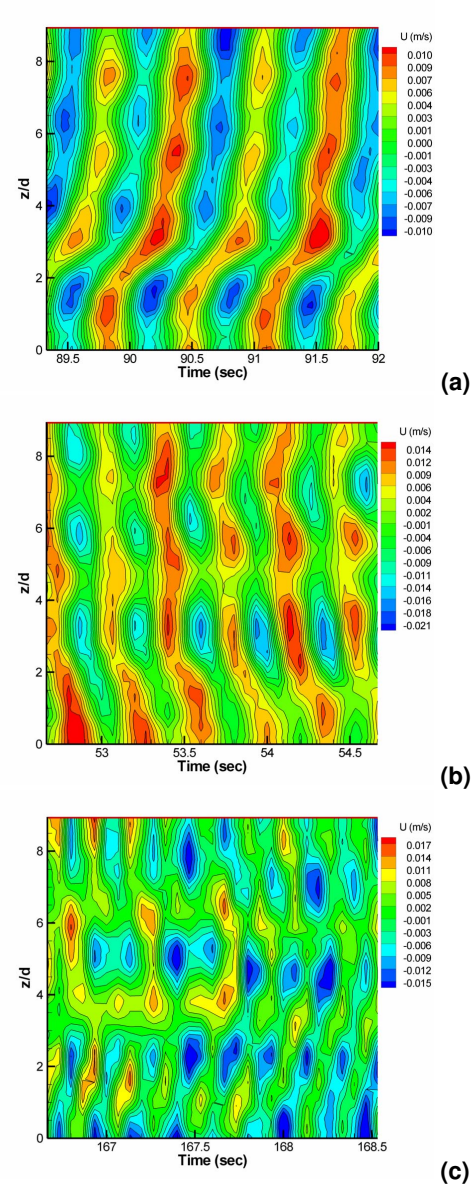

FIGURE 12. SPATIAL AND TEMPORAL VARIATIONS OF U-VELOCITY AT x/d=2.0, y/d=0, BASED ON THE FIRST 32 POD MODES, FOR Re(d)=550 (a), 850 (b), AND 1200 (c)

The spanwise wavelength of the three dimensional instabilities (λ_Z) can be determined based on the POD mode shapes which have been used for generating the plots of Fig.12. Fig. 13 shows the spanwise variations of u_X velocity based on the first 32 POD modes at a downstream location approximately similar that of Fig.12, for $\mathrm{Re}(d) = 550$, 850, and 1200. Based on the variations shown in Fig.13, the average spanwise wavelength of the three dimensional instabilities is found to be $\lambda_Z = 2.0$ for $\mathrm{Re}(d) = 550$, and $\lambda_Z = 2.4$ for $\mathrm{Re}(d) = 850$ and 1200.

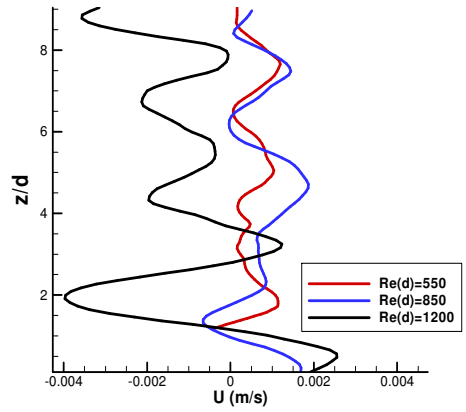

FIGURE 13. SPANWISE VARIATIONS U-VELOCITY AT x/d=2.0, y/d=0, BASED ON THE FIRST 32 POD MODES, FOR Re(d)=550, 850, AND 1200

CONCLUSIONS

The three dimensional instabilities in the wake of blunt trailing edge profiles body, comprising an elliptical leading edge and a rectangular trailing edge, have been studied numerically using 3D unsteady CFD simulations, and experimentally using LIF flow visualizations and PIV measurements of the velocity field in conjunction with the POD technique, at Reynolds numbers ranging from $\mathrm{Re}(d) = 500$ to $\mathrm{Re}(d) = 1200$. The results indicate that for all Reynolds numbers studied herein, the three dimensional instabilities initiate as streamwise dislocations in the von Kármán vortices near the trailing edge, which evolve into pairs of counter-rotating streamwise vortices further downstream. The spanwise wavelength of the three dimensional instabilities (λ_z) has been determined in the near wake region for each case, as described in the previous section, and the results are summarized in Table 1.

TABLE 1. SPANWISE WAVELENGTH OF THE THREE-DIMENSIONAL INTABILITIES (λ_Z)

Numerical		Experimental		
Re(d)	λ_Z/d	Re(d)	λ_Z/d (LIF)	λ_Z/d (PIV)
500	2.0	550	2.1	2.0
800	2.0	850	n/a	2.4
1200	2.5	1200	n/a	2.4

The experimental and numerical values of λ_z found at $\mathrm{Re}(d) = 500 \sim 550$ are in close agreement with the value of $\lambda_z / d = 2.2$ predicted for the same geometry by Ryan et al. [7], based on their stability analysis. The value found at higher Reynolds numbers are very close to the value of $\lambda_z / d = 2.4$, reported in [5] for a square cylinder at $\mathrm{Re}(d) = 2.2 \times 10^4$ and the same value reported in [6] for a blunt trailing edge airfoil at $\mathrm{Re}(d) = 1.3 \times 10^4$. The findings of the present study extend the range of Reynolds numbers at which the three dimensional instabilities in the wake of the blunt trailing edge profiled body are characterized, and can serve as a basis for designing flow control mechanisms that are able to retain their effectiveness in a broader range of operating conditions, by inducing three dimensional instabilities at the appropriate wavelength for each Reynolds numbers.

Finally, it should be noted that the wavelengths mentioned herein are average values, and as one can clearly observe in case of the numerical and experimental results at $\mathrm{Re}(d) = 1200$ (Figs. 8c and 12c, respectively), the wavelength of the three dimensional instabilities is not constant in time, especially at higher Reynolds numbers. The non-uniform spanwise wavelength and the long period variations of λ_z can be attributed to the large-scale low-frequency modulations of the von Kármán vortex street. According to Williamson [2], these large-scale low-frequency modulations, which appear as large-scale spot-like vortex dislocations caused by local shedding phase dislocations across the span, may be caused by several factors, including the effects of the end conditions, and the onset of the transition of the wake into a turbulent one.

REFERENCES

[1] Oertel, Jr., H., 1990, "Wakes behind Blunt Bodies", Annu. Rev. Fluid Mech., **22**, pp. 539-564.

[2] Williamson, C. H. K., 1996, "Vortex Dynamics in the Cylinder Wake", Annu. Rev. Fluid Mech., **28**, pp. 477-539.

[3] Brede, M., Eckelmann, H, and Rockwell, D., 1996, "On Secondary Vortices in the Cylinder Wake", Phys. Fluids, **8**(8), pp. 2117-2124.

[4] Julien, S., Lasheras, J., and Chomaz, J. M., 2003, "Three-dimensional Instability and Vorticity Patterns in the Wake of a Flat Plate", J. Fluid Mech., **479**, pp. 155-189.

[5] Dobre, A., Hangan, H., 2004, "Investigation of the Three-dimensional Wake Topology for a Square Cylinder at High Reynolds Number", Experiments in Fluids, **37**, pp. 518-530

[6] El-Gammal, M., and Hangan, H., 2008, "Three-dimensional Wake Dynamics of a Blunt and Divergent Trailing Edge Airfoil", Experiments in Fluids, **44**, pp. 705-717.

[7] Ryan, K., Thompson, M. C., and Hourigan, K., 2005, "Three-dimensional Transition in the Wake of Bluff Elongated Cylinders", J. Fluid Mech., **538**, pp. 1-29.

[8] Bearman, P. W., and Tombazis, N., 1993, "The Effect of Three-Dimensional Imposed Disturbances on Bluff Body

Near Wake Flows", *J. Wind Eng. and Industrial Aerodynamics*, **49**(1-3), pp. 339-350.

[9] Tombazis, N., and Bearman, P. W., 1997, "A Study of Three-Dimensional Aspects of Vortex Shedding from a Bluff Body with a Mild Geometric Disturbance", J. Fluid Mech., **330**, pp. 85-112.

[10] Park, H., Lee, D., Jeon, W., Hahn, S., Kim, J., Choi, J., and Choi, H., 2006, "Drag Reduction in Flow over a Two-dimensional Bluff Body with a Blunt Trailing Edge Using a New Passive Device", J. Fluid Mech., **563**, pp. 389-414.

[11] Doddipatla, L.S., Hangan, H., Durgesh, V., and Naughton, J.W., 2009, "Passive Flow control of a Flat Plate with Trailing Edge Spanwise Sinusoidal Perturbation", *Proc. ASME 2009 Fluid Engineering Division Summer Meeting (FEDSM 2009),* Vail, Colorado, USA.

[12] Anon., 2005, *Fluent 6.2 User's Guide*, Fluent Inc., Lebanon, NH, USA, Chap. 26.

[13] Holmes, P., Lumley, J.L., Berkooz, G., 1996, *Turbulence, Coherent Structures, Dynamical Systems, and Symmetry*, Cambridge University Press, Cambridge, UK, Chap. 3.

[14] Smith, T.R., Moehlis, J., Holmes, P., 2005, "Low-dimensional Modelling of Turbulence Using the Proper Orthogonal Decomposition: A Tutorial", Nonlinear Dynamics, **41**, pp. 275-307.

[15] Shlens, J., 2009, "A Tutorial on Principal Component Analysis", Salk Institute for Biological Studies, available online at: http://www.snl.salk.edu/~shlens/#pubs